Julia L. Gregory, Anne Walter, Yannick O. Alexandre, Jyh Liang Hor, Ruijie Liu, Joel Z. Ma, Sapna Devi, Nobuko Tokuda, Yuji Owada, Laura K. Mackay, Gordon K. Smyth, William R. Heath, and Scott N. Mueller

Infection programs sustained lymphoid stromal cell responses and shapes lymph node remodeling upon secondary challenge

Cell Reports, 2017; 18(2):406-418

Originally published at:
http://doi.org/10.1016/j.celrep.2016.12.038

Article

Cell Reports

Infection Programs Sustained Lymphoid Stromal Cell Responses and Shapes Lymph Node Remodeling upon Secondary Challenge

Graphical Abstract

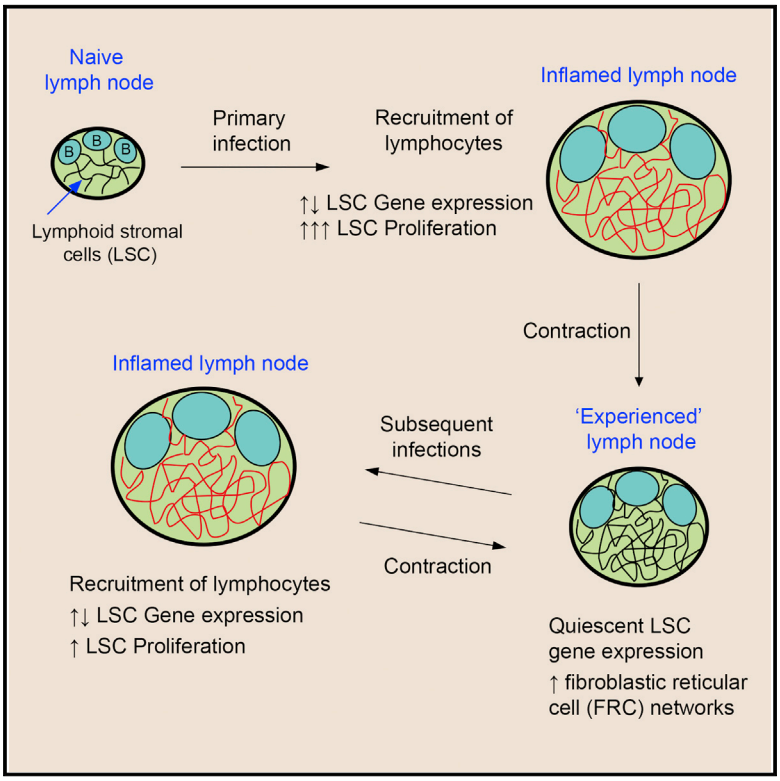

Highlights

- Infection induces a robust transcriptional program in lymphoid stromal cells (LSCs)
- The LSC transcriptional program is not sustained after resolution of infection
- Prolonged LSC expansion occurs after infection that is sustained by B cells
- Experienced LSC networks support subsequent immune responses via reduced expansion

Authors

Julia L. Gregory, Anne Walter, Yannick O. Alexandre, ..., Gordon K. Smyth, William R. Heath, Scott N. Mueller

Correspondence

smue@unimelb.edu.au

In Brief

Lymph nodes are constructed of intricate networks of stromal cells. Gregory et al. reveal a robust yet transient transcriptional program in lymph node stromal cells induced by virus infection. Previously primed lymph nodes sustained amplified networks of stromal cells that supported subsequent immune responses.

Accession Numbers

GSE84284

Gregory et al., 2017, Cell Reports *18*, 406–418
January 10, 2017
http://dx.doi.org/10.1016/j.celrep.2016.12.038

CellPress

OPEN ACCESS
CellPress

Cell Reports
Article

Infection Programs Sustained Lymphoid Stromal Cell Responses and Shapes Lymph Node Remodeling upon Secondary Challenge

Julia L. Gregory,[1] Anne Walter,[1] Yannick O. Alexandre,[1] Jyh Liang Hor,[1,2] Ruijie Liu,[3] Joel Z. Ma,[1] Sapna Devi,[1,2] Nobuko Tokuda,[4] Yuji Owada,[5] Laura K. Mackay,[1] Gordon K. Smyth,[3,6] William R. Heath,[1,2] and Scott N. Mueller[1,2,7,*]

[1]Department of Microbiology and Immunology, The University of Melbourne, Peter Doherty Institute for Infection and Immunity, Melbourne, VIC 3000, Australia
[2]The Australian Research Council Centre of Excellence in Advanced Molecular Imaging, University of Melbourne, VIC 3000, Australia
[3]Bioinformatics Division, The Walter and Eliza Hall Institute of Medical Research, 1G Royal Parade, Parkville, VIC 3052, Australia
[4]Faculty of Health Sciences, Yamaguchi University Graduate School of Medicine, 1-1-1 Minami-Kogushi, Ube 755-8505, Japan
[5]Department of Organ Anatomy, Tohoku University Graduate School of Medicine, 2-1 Seiryo-machi, Sendai 980-8575, Japan
[6]Department of Mathematics and Statistics, The University of Melbourne, Parkville, VIC 3010, Australia
[7]Lead Contact
*Correspondence: smue@unimelb.edu.au
http://dx.doi.org/10.1016/j.celrep.2016.12.038

SUMMARY

Lymph nodes (LNs) are constructed of intricate networks of endothelial and mesenchymal stromal cells. How these lymphoid stromal cells (LSCs) regulate lymphoid tissue remodeling and contribute to immune responses remains poorly understood. We performed a comprehensive functional and transcriptional analysis of LSC responses to skin viral infection and found that LSC subsets responded robustly, with different kinetics for distinct pathogens. Recruitment of cells to inflamed LNs induced LSC expansion, while B cells sustained stromal responses in an antigen-independent manner. Infection induced rapid transcriptional responses in LSCs. This transcriptional program was transient, returning to homeostasis within 1 month of infection, yet expanded fibroblastic reticular cell networks persisted for more than 3 months after infection, and this altered LN composition reduced the magnitude of LSC responses to subsequent heterologous infection. Our results reveal the complexity of LSC responses during infection and suggest that amplified networks of LN stromal cells support successive immune responses.

INTRODUCTION

The secondary lymphoid organs function as a surveillance network to capture pathogens and initiate immune responses. The organized microarchitecture of lymph nodes (LNs) facilitates interactions by immune cells within a complex network of endothelial and mesenchymal stromal cells (Brown and Turley, 2015; Fletcher et al., 2015; Mueller and Germain, 2009). LNs are encapsulated structures through which lymph is filtered, entering the LN subcapsular sinus that connects to the cortical and medullary lymphatics. Lymphocytes migrating through an LN enter the lymphatic sinuses, where they can proceed to the next LN in the lymphatic chain and ultimately re-enter the bloodstream via the thoracic duct. T cells that enter LNs via afferent lymphatics, either from tissues or upstream LNs, can enter via medullary sinuses, whereas dendritic cells (DCs) that migrate from the tissues are able to cross the lymphatic floor of the subcapsular sinus (SCS) (Schulz et al., 2016). Cells that enter LNs from the blood do so via specialized blood vessels composed of phenotypically distinct blood endothelial cells (BECs). These high endothelial venule (HEV) cells express molecules required for cells to enter LNs, including peripheral node addressin (PNAd). HEVs are concentrated in certain areas of LNs, particularly in the outer paracortex (cortical ridge) between the T and B cell zones.

Networks of mesenchymal stromal cells construct and define the boundaries of the different compartment of LNs. Fibroblastic reticular cells (FRCs) are found in T cell zones, where they produce and ensheath collagen-rich reticular fibers and construct a conduit network through which small molecules can filter into LNs (Gretz et al., 2000; Sixt et al., 2005). T cell zone FRCs are defined by expression of markers, including gp38 (podoplanin), and production of homeostatic cytokines (interleukin 7 [IL-7]) and chemokines (CCL21 and CCL19) that are required for lymphocyte migration and homeostasis (Mueller and Germain, 2009). FRCs are also found within the LN medulla. Another subset of gp38^{+} mesenchymal stromal cells forms a network underneath the SCS adjacent to B cell follicles. These marginal reticular cells (MRCs) express many markers of other stromal cells, as well as mucosal vascular addressin cell adhesion molecule 1 (MADCAM-1) and high levels of the receptor activator of nuclear factor κB (NF-κB) ligand (RANKL). Within B cell zones, follicular dendritic cells (FDCs) form a dense network in the follicle center, whereas other B cell zone reticular cells (BRCs) construct the follicle boundaries. Both FDCs and BRCs express the chemokine CXCL13, while FDCs express Fc receptors (such

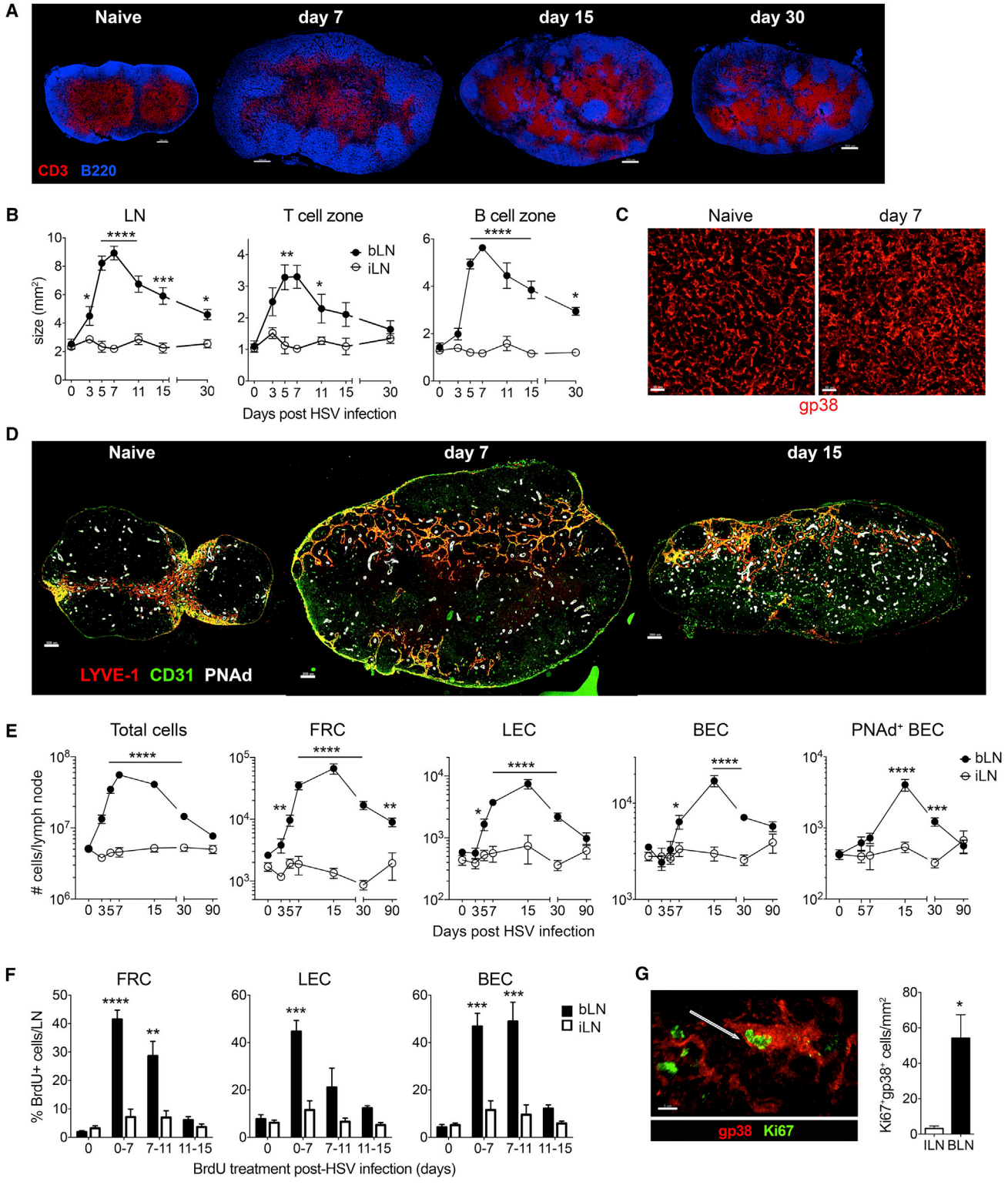

Figure 1. Lymphoid Stromal Cell Responses to Infection

(A) Immunofluorescence staining of medial bLN sections for CD3 and B220 at different times after skin HSV infection.

(B) Quantitation of bLN and non-draining inguinal lymph node (iLN) sections for total area and T and B cell zone regions. n = 4–6 mice per time point.

(C) gp38 staining in the T cell zone of bLNs of uninfected mice and 7 days after HSV infection.

(legend continued on next page)

as CD16 and CD32), complement receptors (CD21 and CD35), and complement components.

The lymphoid stromal cell (LSC) subsets have been shown to influence immunity and contribute to T cell responses in several ways. In addition to lymphocyte migration and homeostasis (Bajénoff et al., 2008; Link et al., 2007; Luther et al., 2000), FRCs can induce peripheral T cell tolerance (Baptista et al., 2014; Dubrot et al., 2014; Fletcher et al., 2010) and restrict T cell proliferation (Khan et al., 2011; Lukacs-Kornek et al., 2011; Siegert et al., 2011). Moreover, deletion of CCL19-expressing LSCs demonstrated a critical role for intact LSC networks for lymphocyte and dendritic cell homeostasis (Cremasco et al., 2014). Recent elegant studies also demonstrated functional roles for gp38 expressed on LSCs for DC migration through engagement of the C-type lectin domain family 1 member B (CLEC2) and for inhibiting FRC contractility via CLEC2 binding (Acton et al., 2012, 2014; Astarita et al., 2015). This latter observation suggests that FRC networks in LNs might stretch to accommodate increases in cellularity induced rapidly by inflammation. Following immunization of mice with ovalbumin in complete Freund's adjuvant (OVA/CFA), the major subsets of LSCs were shown to proliferate to control LN growth (Abe et al., 2014; Chyou et al., 2011; Yang et al., 2014). Similarly, infections induce substantial hypertrophy of draining LNs. However, what signals control these LSC responses, whether these are tailored to the inflammatory milieu induced by different pathogens, and how LSCs respond to infection at the molecular level are not known.

In this study, we examined responses by LN FRC, lymphatic endothelial cell (LEC), and BEC populations to skin virus infection. The LSCs responded rapidly and robustly to infection, proliferating and significantly modulating gene expression. We show that expansion of FRC networks was long-lived, but the transcriptional program induced by infection was transient. Primary infection with different viral pathogens induced distinct patterns of LSC expansion, yet all induced sustained remodeling that altered responses induced by a subsequent infection. Thus, we provide insight into the cellular and molecular mechanisms driving the remodeling of LN LSCs during primary and secondary immune challenges.

RESULTS

LN Remodeling and Expansion of LSCs after Cutaneous HSV Infection

To begin to examine how LNs are remodeled during infection to support the generation of the immune response, we utilized a well-established model of localized skin infection with herpes simplex virus type 1 (HSV-1). Mice infected on the flank prime adaptive immune responses in the primary draining brachial LN (bLN). HSV-1 is an acute infection that is cleared from the skin of mice within 1 week and remains latent in dorsal root ganglia. We have shown that priming of T cell responses after skin HSV-1 infection is rapid and involves an increase in the size of the draining bLN within days (Hor et al., 2015). Visualization of medial bLN sections by microscopy confirmed a marked increase in bLN size (Figures 1A and 1B), which reached a maximum at 1 week after infection. This ~4-fold increase in bLN cross-sectional area contracted after day 7 yet remained increased for more than 30 days compared to non-draining LN. Measurement of T and B cell regions by co-staining for CD3 and B220 revealed similar kinetics of expansion in volume of these compartments, with B cell zones remaining enlarged 30 days after infection (Figure 1B).

The gp38$^+$ stromal network in bLNs was increased in size corresponding to the enlarged T cell zones. On day 7, the gp38$^+$ network in the T cell zones was less organized and denser, but it did not appear disrupted or overtly damaged (Figure 1C). gp38$^+$ cells within the medulla also expanded appreciably after infection (Figure S1A). These nodular regions were surrounded by LYVE-1$^+$ lymphatics and contained T and B cells as well as blood vessels that were mostly PNAd$^+$ HEVs. We also examined changes in the blood and lymphatic vasculature. LYVE-1$^+$ lymphatic structures were increased and there was marked expansion of LN blood vessels, in particular PNAd$^+$ HEVs, on day 15 after infection (Figure 1D).

To enumerate populations of stromal cells in bLNs we enzymatically digested individual LNs after HSV-1 infection. Single-cell suspensions were stained for gp38 and CD31 to identify the major LN stromal cell subsets among CD45$^-$ cells: FRCs, LECs, and BECs (Figure S1B). We also co-stained BECs for PNAd to identify HEV endothelial cells. Mock infection (skin scarification plus PBS) did not induce LN hypertrophy or an increase in numbers of LSCs in bLNs (Figure S1C). After HSV infection, total cellularity in bLNs increased significantly within 3 days, peaking by day 7 and gradually contracting, yet it remained increased for at least 1 month (Figure 1E). T and B cell and DC numbers in bLNs peaked by day 7 after infection, contracted slowly, and remained marginally increased at day 30 but returned to pre-infection levels by day 90 (Figure S1D). Expansion of bLN FRCs was slightly delayed compared with total cellularity, beginning at day 5 and peaking by day 15 at levels >20-fold higher than in uninfected LNs (Figure 1E). Although the bLN FRC compartment contracted after day 15, numbers of FRCs remained significantly increased for at least 3 months after infection. This suggested that remodeling of the LN FRC compartment was sustained after peripheral viral infection. Similarly, LECs expanded >10-fold after infection, peaking at day 15, and remained elevated for at least 1 month. BECs expanded later than FRCs and LECs, with

(D) Immunofluorescence staining of bLNs for CD31, PNAd, and LYVE-1 to identify blood vessels (CD31$^+$), HEVs (CD31$^+$ PNAd$^+$), and lymphatic vessels (CD31$^+$ LYVE-1$^+$) at different times after skin HSV infection.

(E) Analysis of cell populations in bLN and non-draining iLN by flow cytometry after HSV infection. n = 6–24 mice per time point.

(F) Proliferation of LSC subsets after HSV infection. Mice were treated with BrdU in drinking water for the indicated periods of days after infection. n = 5–8 mice per time point.

(G) Upregulation of Ki67 in gp38$^+$ FRCs after infection. bLN sections were stained for gp38 and Ki67. n = 4–5 mice.

Error bars represent mean ± SEM. *p < 0.05, **p < 0.01, ***p < 0.001, and ****p < 0.0001 by one-way ANOVA with Holm-Sidak's multiple-comparisons test (B) or Kruskal-Wallis test followed by Dunn's multiple-comparisons test (E and F). *p = 0.0159 by two-tailed Mann-Whitney test (G). See also Figure S1.

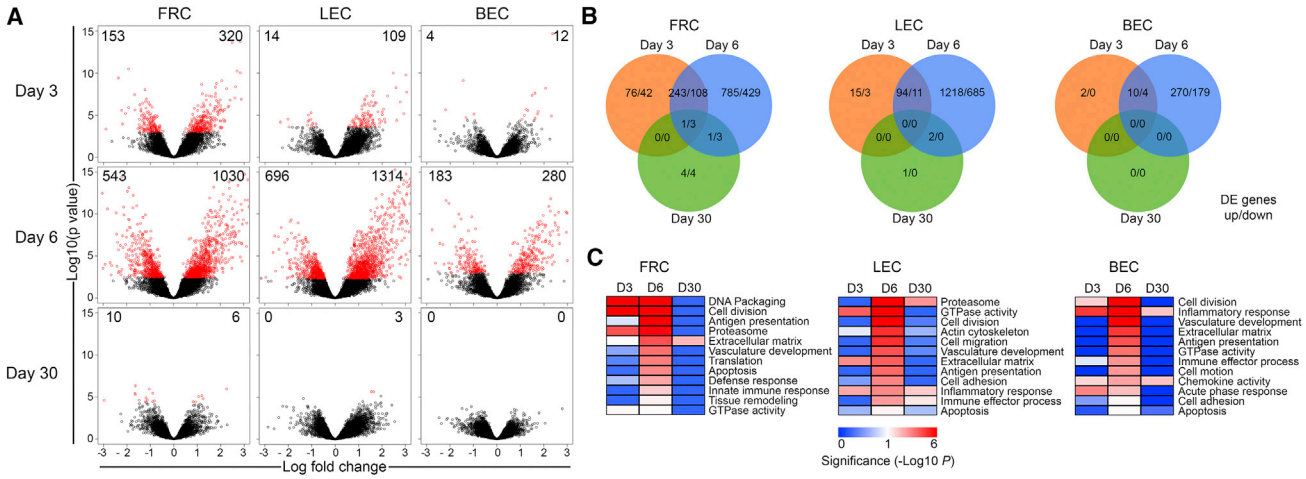

Figure 2. Gene Expression Changes in LSC Subsets Induced by Infection

(A) Volcano plots of FRCs, LECs and BECs from bLN 3, 6, and 30 days after HSV infection showing differentially expressed genes compared to uninfected mice. Differentially expressed genes are shown in red. Numbers refer to number of genes either downregulated (top left) or upregulated (top right) in each comparison.

(B) Comparison of differential gene expression within each LSC subset at different time points after HSV infection. Numbers represent genes up/downregulated in each comparison.

(C) GO term enrichment in FRCs, LECs or BECs at day 6 compared to cells from uninfected mice.

See also Figure S2.

a lower magnitude (4-fold), yet also peaked in number at day 15. The PNAd$^+$ subset of BECs expanded substantially after day 7 (~8-fold), reflecting the large number of PNAd$^+$ vessels observed in bLN sections at day 15 (Figure 1D). In contrast, the CD45$^-$CD31$^-$gp38$^-$ (double negative [DN]) population, which consists of pericytes and other unidentified LN stromal cells (Malhotra et al., 2012), peaked at day 7 before contracting to baseline within 30 days (Figure S1D).

Each of the three main LSC subsets proliferated robustly after HSV infection, with 40%–50% of FRCs, LECs, and BECs incorporating bromodeoxyuridine (BrdU) within the first week (Figure 1F). Confocal microscopy on sections from bLN 6 days after infection revealed substantial numbers of gp38$^+$ Ki67$^+$ cells, indicating proliferation (Figure 1G). These Ki67$^+$ gp38$^+$ cells were distributed throughout the bLNs as opposed to foci of expanding cells. After day 7, FRCs and LECs showed reduced BrdU uptake, indicating that much of the proliferation of these cells occurred within the first week of the infection. In contrast, BECs continued to proliferate until day 11 (Figure 1F). Concomitant with expansion, FRCs showed marked upregulation of gp38, which peaked 1 week after infection and returned to baseline within 30 days (Figure S1E). Together these data demonstrate that LN stromal cells respond robustly to peripheral virus infection and maintain an enlarged LN microenvironment for prolonged periods after clearance of infection.

Prominent Transcriptional Changes in LSC Subsets Induced after Infection

To investigate gene expression changes in FRCs, LECs, and BECs throughout the course of peripheral infection we sorted these LSC subsets to high purity from bLNs obtained from naive mice and mice infected with HSV 3, 6, and 30 days previously (Figure S2A) and then profiled the RNA samples using Affymetrix microarrays. Principal-coordinate analysis showed that the three LSC subsets have distinct expression profiles and confirmed that the transcriptional identity of these subsets was unchanged by infection (Figure S2B). We examined expression of previously identified genes known to be expressed by each cell subset, confirming the identity of the cells (Figure S2C).

Hierarchical clustering of differentially expressed probes within each LSC subset demonstrated abundant changes in gene expression after infection (Figure S2D). To prioritize the most important genes, we assessed differential expression induced by infection using the TREAT (t tests relative to a threshold) method (McCarthy and Smyth, 2009), which requires fold changes (FCs) to be significantly above a minimum threshold. Using a false discovery rate (FDR) of 5%, we compared gene expression within each subset at various time points after infection to that of uninfected cells of the same cell type. The TREAT method evaluates variability as well as well as the magnitude of change in expression values and therefore is not equivalent to a simple fold change cutoff. Nevertheless, almost all the statistically significant expression changes were greater than 1.5-fold and most were greater than 2-fold. Within 3 days of infection, bLN FRCs up- or downregulated over 470 genes and LECs over 100 genes (Figure 2A). Notably, at this early time point, BECs showed almost no differential gene expression. By day 6 (roughly the peak of the T cell response to HSV), FRCs showed regulation of >1,500 genes (1,030 upregulated and 543 downregulated), while LECs and BECs had >2,000 and >450 differentially expressed (DE) genes, respectively. Remarkably, this response was entirely transient, with gene expression by each subset returning to baseline within 30 days of infection (Figure 2A).

Evaluation of genes regulated during HSV infection within each stromal cell subset revealed that most transcriptional changes that began early (by day 3) continued until day 6, with

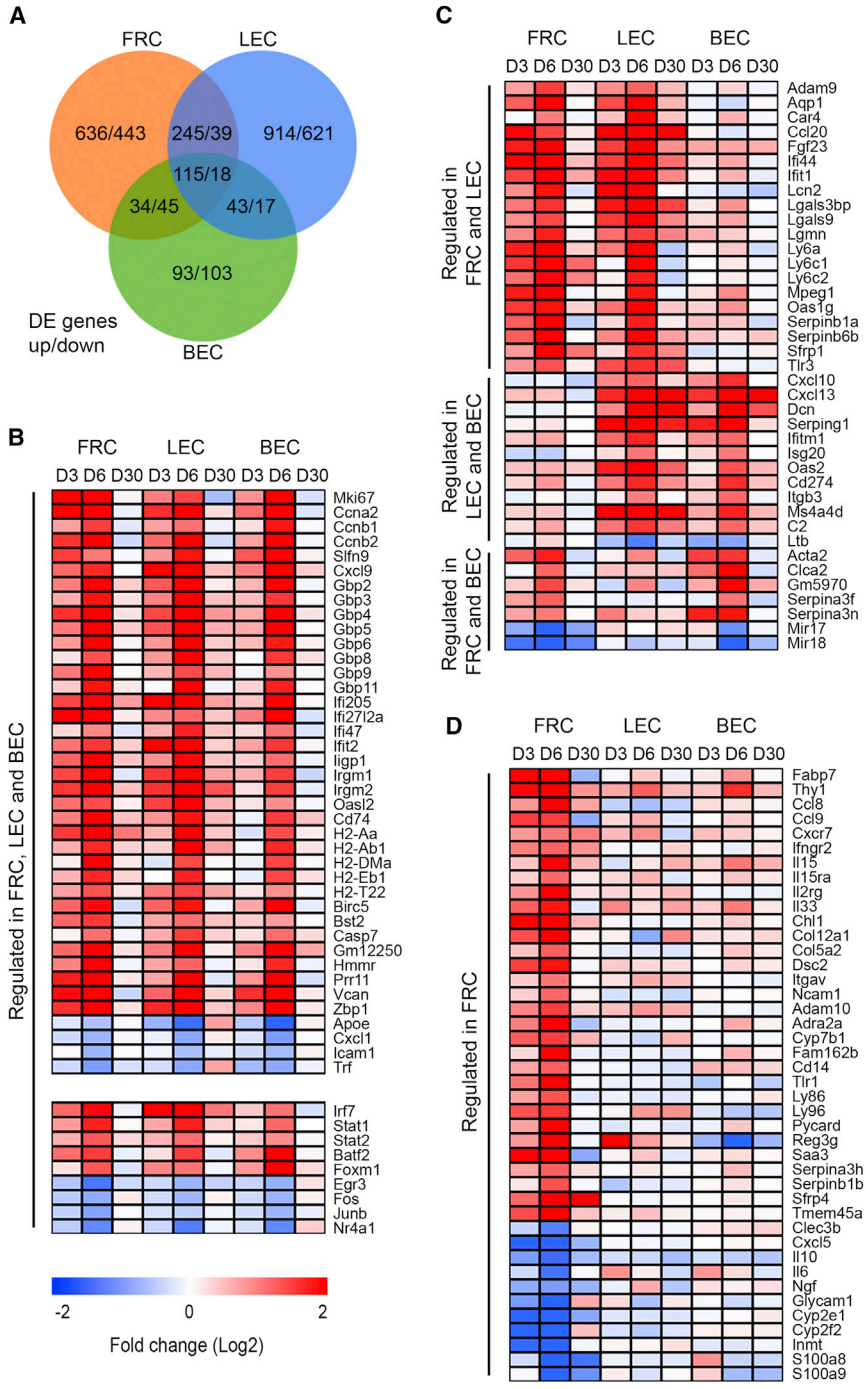

Figure 3. Identification of Genes Regulated in LSC Subsets after Infection

(A) Comparison of differentially expressed genes in FRCs, LECs, and BECs 6 days after HSV infection. Numbers represent genes up- or downregulated in each comparison.

(B–D) Heatmaps depicting log2 expression fold-changes (log2 FCs) of differentially expressed genes in FRCs, LECs, and BECs at different time points after HSV infection. (B) Cohorts of genes regulated similarly in all three LSC subsets at day 6. (C) Cohorts of genes regulated similarly in two of the three LSC subsets. (D) Genes uniquely regulated in FRCs 6 days after infection compared to that in LECs and BEC.

See also Figure S3.

relatively few genes uniquely regulated at day 3 (Figure 2B). Most gene expression regulation occurred between days 3 and 6 (Tables S1 and S2). The DE genes in each LSC subset showed enrichment for similar functional pathways, including cell division, antigen presentation, extracellular matrix, and apoptosis, as well as prominent defense and immune response pathways (Figure 2C).

Comparison of DE genes in FRCs, LECs, and BECs 6 days after infection revealed a cohort of >100 genes regulated significantly in the same direction in all three cell types (Figures 3A and 3B; Table S1). These included multiple genes involved in cell division (e.g., *Mki67*, *Ccna2*, *Ccnb1/2*, *Prr11*, and *Foxm1*), the interferon response (e.g., *Gbp2/3/4/5/6/8/9/11*, *Irgm1/2*, and *Stat1/2*), the chemokine *Cxcl9*, and the transcription factor *Batf2*. Multiple major histocompatibility complex class II (MHC II) genes were upregulated, and staining of cells 7 days after infection confirmed increased MHC II expression by FRCs, LECs and BECs (Figure S4A). The PYHIN protein family member *Ifi205* and the Z-DNA-binding protein 1 (*Zbp1*), which function as DNA sensors, were upregulated in all three subsets of LSCs. Versican (*Vcan*), an extracellular matrix protein that interacts with various partners, including chemokines and hyaluronan, and may regulate cell contractility (Hirose et al., 2001; Wight, 2002), was also significantly upregulated in FRCs, LECs, and BECs. Some genes, including *Apoe*, *Cxcl1*, *Icam1*, and *Trf*, as well as the transcription factors *Egr3*, *Fos*, and *Nr4a1* (Nur77), were uniformly downregulated in the LSC subsets.

We also found that numerous genes were regulated significantly in two of the three LSC subsets (Figure 3C), although this often also involved similar non-significant changes in gene expression in the third LSC subset. These included the Tim-3 ligand galectin-9 (*Lgals9*) the defense gene *Mpeg1*, smooth muscle actin (*Acta2*), interferon-induced genes (including *Oas1g*, *Ifit1*, *Ifitm1*), and the transcription factor *Irf7*. Many genes were coregulated by FRCs and LECs (245 genes). These included *Aqp1, Ccl20, Ly6a* (also known as Sca-1), and the anti-bacterial protein lipocalin-2 (*Lcn2*). In contrast, FRCs and BECs, as well as LECs and BECs, showed coregulation of only

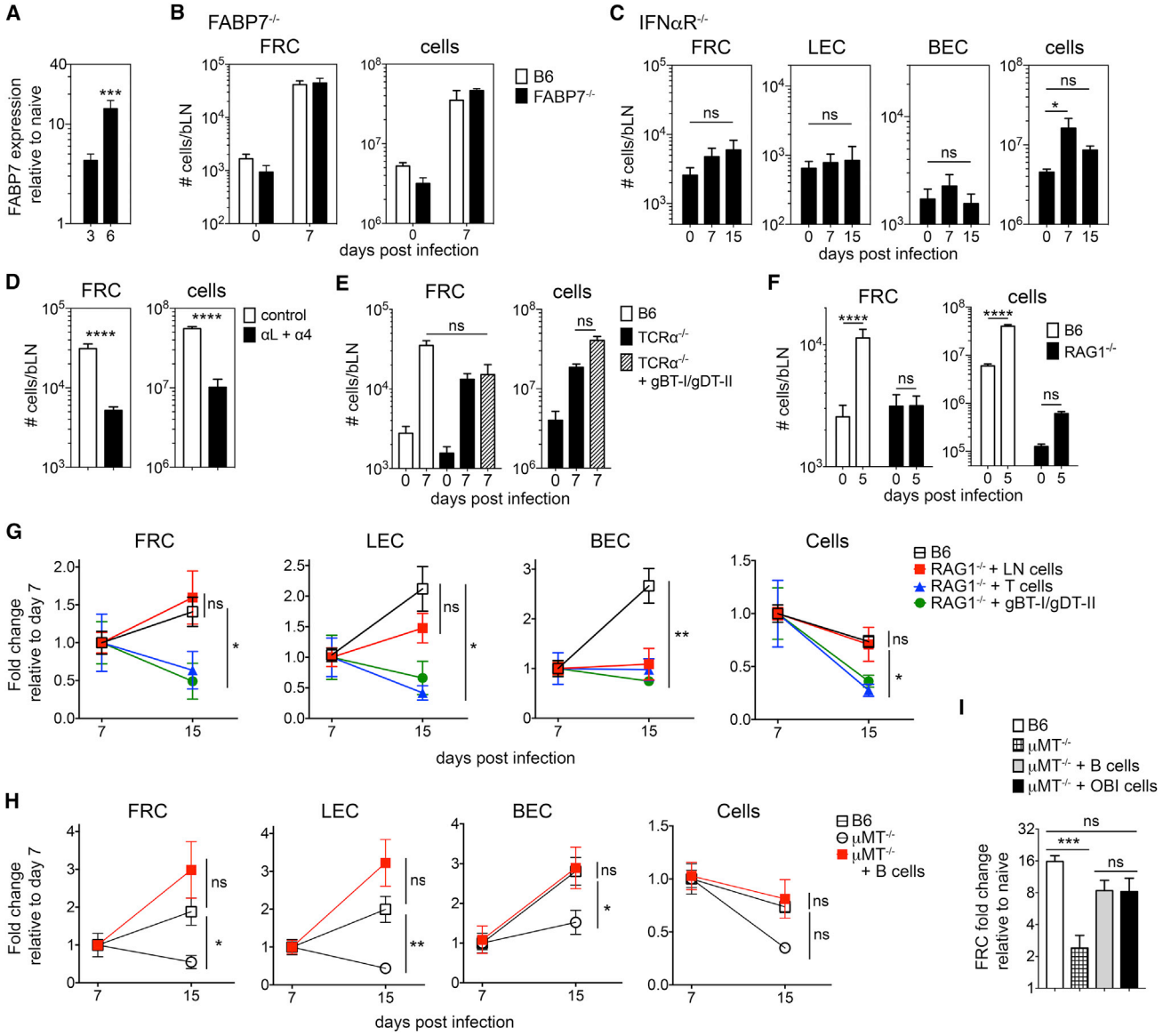

Figure 4. Induction and Maintenance of LSC Expansion after Infection Requires B Cells

(A) Expression of FABP7 mRNA in fluorescence-activated cell sorting (FACS) sorted FRCs 3 and 6 days after HSV infection, determined by RT-PCR. n = 4.

(B) Normal expansion of LSC subsets in the bLN of FABP7$^{-/-}$ mice after HSV infection. n = 5–7 mice per time point.

(C) LSCs do not expand in IFN-αR$^{-/-}$ mice after HSV infection. Mice were transferred with in-vitro-activated gBT-I T cells 3 days after infection to prevent viral spread to the CNS. n = 6 mice per time point.

(D) Blocking T cell recruitment to the bLN inhibits FRC expansion after HSV infection. Mice were treated with anti-αL and anti-α4 antibodies on days 1, 3, and 5 after infection and analyzed at day 7. n = 8 mice per group.

(E) Expansion of the bLN and FRCs is normal in TCR-α$^{-/-}$ mice. Mice were infected with HSV or transferred with 10^6 gBT-I CD8 and gDT-II CD4 T cells prior to infection and analyzed 7 days post-infection. Control mice were uninfected and a control group also transferred with transgenic T cells for 7 days. n = 6–15 mice per group.

(F) Expansion of bLNs and FRCs is impaired in RAG1$^{-/-}$ mice. Mice were infected with HSV and analyzed 5 days post-infection. n = 13–14 mice per group.

(G) T cells induce LSC expansion in RAG1$^{-/-}$ mice after HSV infection that contracts after day 7. RAG1$^{-/-}$ mice were transferred with 2×10^7 non-enriched B6 LN cells, 2×10^7 enriched naive T cells, or 10^6 naive gBT-I and gDT-II T cells prior to HSV infection. LSCs were analyzed in bLN 7 and 15 days later. Shown are the fold changes in LSC numbers at day 15 relative to day 7. n = 6 mice per group.

(H) B cells sustain LSC numbers in μMT$^{-/-}$ mice after HSV infection. μMT$^{-/-}$ mice in one group were transferred with 2×10^7 enriched naive B cells prior to infection. Control mice were uninfected and also received transferred cells for 7 or 15 days. Shown are the fold changes in LSC numbers at day 15 relative to day 7. n = 6–11 mice per group.

(legend continued on next page)

small cohorts of genes (71 and 50 genes, respectively). LECs and BECs both upregulated the chemokines *Cxcl10* and *Cxcl13*, the decorin protein (*Dcn*) that can regulate cell cycle, and the C1-inhibitor *Serping1*. *Thy1* was also upregulated in all LSC subsets, although significantly only in FRCs. Staining of cells ex vivo revealed that a proportion of FRCs and LECs upregulated Thy1 after infection (Figure S4A).

Many genes were upregulated uniquely in FRCs after infection (986 genes). These included *Ifngr2*, *Il2rg*, *Il15ra*, *Il15*, *Il33*, *Tmem173* (STING), *Ccl8*, and *Ccl9* (Figure 3D; Table S1). Other genes highly upregulated in FRCs included fatty-acid-binding protein *Fabp7*; the adhesion molecules *Chl1*, *Dsc2*, and *Ncam*; the acute phase response protein *Saa3*; the receptor *Timd4*; and the adrenergic receptor *Adra2a*. The anti-angiogenic molecule tissue inhibitor of metalloproteinase 1 (*Timp1*) was upregulated in FRCs, suggesting that this might regulate responses by BECs after infection (Zanotti et al., 2016). The transcription factors *Batf3* and the vitamin D receptor (*Vdr*) were also upregulated uniquely in FRCs (Figure S3A). A similar number of genes were downregulated in FRCs, including *Cxcl5*, *Il10*, *Il6*, *Glycam1*, *S100a8*, and *S100a9*, and transcription factors, including *Id3* and *Klf2*.

As previously described (Mueller et al., 2007), expression of the homeostatic chemokine CCL21 in the draining bLN was significantly reduced after infection (Figure S4B). We could not detect regulation within our gene expression profiles, presumably due to saturation of the highly abundant *Ccl21a* transcripts in the microarrays. However, significant downregulation of *Ccl21* mRNA was observed by qRT-PCR in sorted FRCs 3 and 6 days after infection (Figure S4B). Thus, activation of FRCs by infection resulted in decreased expression of CCL21.

The bLN LECs upregulated a very large cohort of unique genes (1,390 genes), including *Il7*, *Ccl2*, *Ccl5*, *Ccl7*, *Ccl21a*, *Tlr13* and downregulated molecules, including *Cd226* (DNAM-1) and *Marco* (Figure S3B). In comparison, bLN BECs only regulated a relatively modest cohort of unique genes (188 genes), including upregulation of *Cxcl11*, complement component 3 (*C3*), and *Vegfc* and downregulation of *Ccr7*, *Cxcr4*, and the adrenergic receptor *Adrb2* (Figure S3C). Thus, LSCs responded rapidly and robustly to peripheral infection, suggesting complex regulation of gene expression by LSCs in response to infection. However, this transcriptional program was transient, as gene expression in these cells 30 days after infection was indistinguishable to that in uninfected cells.

Lymphocytes Induce and Sustain LSC Responses to Infection

The prominent changes in gene expression by the LSC subsets after HSV infection led us to examine the signals required for expansion of these cells. Our transcriptional profiling revealed marked upregulation of *Fabp7*, and we confirmed this change by qRT-PCR in sorted FRCs (Figure 4A). Since Fabp7 has been suggested to play a role in the expansion of astrocytes and some cancer cells (Sharifi et al., 2011), we wanted to determine whether this protein was involved in the proliferation of FRCs after infection. Fabp7$^{-/-}$ mice were infected with HSV and numbers of FRCs examined in bLNs. We did not detect any deficiency in the architecture of bLNs in these mice, and expansion of FRCs was unaffected compared with wild-type mice (Figure 4B). We also examined the role of various innate immune sensors and signals that can contribute to immune responses to HSV, using mice deficient in interleukin 1 converting enzyme (ICE), Trif, MyD88, toll like receptor 3 (TLR3), IL-15, and interferon γ (IFN-γ). FRCs in each of these mice expanded like control mice (Figure S4C). Similarly, mice lacking interferon regulatory factor 8 (IRF8), which have deficiencies in CD8α and CD103$^+$ dendritic cell populations, demonstrated normal expansion of FRCs.

The type I interferon (IFN-I) signature induced by infection in the LSC subsets led us to ask whether IFNαR signals were required for stromal expansion. IFN-αR2$^{-/-}$ mice infected with HSV showed no LSC expansion on days 7 and 15 (Figure 4C). Importantly, total cellularity in bLNs of IFN-αR2$^{-/-}$ mice increased minimally after HSV infection, indicating that cell recruitment or retention in the LN was required for stromal cell expansion. To examine this directly, we treated mice with neutralizing antibodies to αL and α4 integrins to block LN entry, beginning 24 hr after infection. This inhibited the accumulation of cells in the bLN and resulted in significantly reduced expansion of FRCs (Figure 4D), demonstrating that lymphocyte recruitment to bLNs was critical for LSC expansion after infection.

Expansion of the bLNs or FRCs was not significantly impaired in TCR-$\alpha^{-/-}$ mice, which lack mature T cell receptor $\alpha\beta$-positive (TCR-$\alpha\beta^+$) T cells (Figure 4E). Transfer of HSV-specific CD4$^+$ gDT-II and CD8$^+$ gBT-I T cells into TCR-$\alpha^{-/-}$ mice prior to infection also did not alter FRC expansion, suggesting that antigen-specific T cell recruitment or expansion was not required to induce LSC growth after infection. In contrast, when we examined responses in lymphocyte-deficient RAG$^{-/-}$ mice, we found that expansion of the stromal cells was completely abrogated (Figure 4F). To determine whether we could reconstitute expansion of the LN stromal compartment, RAG$^{-/-}$ mice were adoptively transferred with 2×10^7 total LN cells from B6 mice, 2×10^7 polyclonal T cells, or 1×10^6 gDT-II and gBT-I T cells and then infected with HSV on the skin. Control mice were left uninfected and analyzed 7 or 15 days after cell transfer. Reconstitution of RAG$^{-/-}$ mice did not induce expansion of the bLN LSCs in the absence of infection, but it facilitated expansion after HSV infection. Transfer of unenriched LN cells, polyclonal T cells, or low numbers of HSV-specific T cells all triggered robust LSC responses (Figure S5A). Although bLNs from RAG$^{-/-}$ mice were smaller and contained fewer LSCs than bLNs from B6 mice, the magnitude of LSC expansion was similar or greater in RAG$^{-/-}$ mice 7 days after infection. This suggested that the

(I) Antigen non-specific B cells can sustain FRCs expansion after infection. Mice were treated as in (H), with an additional group of mice transferred with 2×10^7 naive B cells from OBI-RAG$^{-/-}$ mice. n = 6–14 mice per group. Data are pooled from two or three independent experiments.

Error bars represent mean ± SEM. *p < 0.05, **p < 0.01, ***p < 0.001, and ****p < 0.0001 by one-way ANOVA with Dunnett's multiple-comparisons test (A–C), by two-tailed Mann-Whitney test (D), by Kruskal-Wallis test followed by Dunn's multiple-comparisons test (E and G–I), or by two-way ANOVA with Bonferroni's multiple-comparisons test (F). See also Figures S4 and S5.

transferred cells were capable of triggering LSC expansion. However, in mice receiving polyclonal or transgenic T cells, these responses were not sustained, and by day 15 after infection, LSCs in these mice contracted (Figure 4G). In contrast, transfer of total LN cells promoted sustained expansion of FRCs and LECs from days 7 to 15.

Since our results suggested that T cells were not required yet were sufficient to induce expansion of the bLN stromal populations after infection, we examined responses in $\mu MT^{-/-}$ mice that lack mature B cells but have normal numbers of T cells. Although LSCs expanded in $\mu MT^{-/-}$ mice, after day 7, numbers of FRCs and LECs contracted, and BECs failed to expand further, unlike B6 mice, where LSC expansion peaked at day 15 (Figures 4H and S5B). This inability to sustain LSC expansion suggested a role for B cells in this process. To examine this, we reconstituted $\mu MT^{-/-}$ mice with polyclonal B cells from B6 mice prior to HSV infection. Expansion of the LSCs at day 7 in these mice was similar to $\mu MT^{-/-}$ mice not given B cells. Transfer of B cells induced sustained LN expansion (Figures 4H and S5B). Notably, while the transfer of polyclonal T or B cells induced a similar increase in bLN cellularity (Figure S5C), only B cells sustained LSC expansion. Moreover, transfer of ovalbumin-specific B cells from OBI-$RAG^{-/-}$ mice (Dougan et al., 2012) demonstrated that B cells sustained FRC expansion in a non-specific manner (Figure 4I). These data show that either B cells or T cells were sufficient to trigger LSC expansion, yet B cells were required to sustain stromal cell responses.

Sustained LSC Expansion Influences Secondary Responses

The protracted expansion of the LSC subsets after HSV infection could reflect a programmed response that is induced by inflammation, influenced by the pathogen, or both. To investigate the kinetics of LSC responses to different viral infections, we examined proliferation in response to skin infection with HSV, vaccinia virus (VV), or lymphocytic choriomeningitis virus (LCMV). Surprisingly, the kinetics of FRC expansion was different for each pathogen (Figure 5A). Compared to HSV infection, skin VV infection induced a peak of FRC expansion by day 7, followed by contraction by day 15. In contrast, skin LCMV infection induced delayed FRC expansion that peaked around day 15 and did not contract. Despite different growth and contraction kinetics, all three infections induced prolonged expansion of FRCs. At day 30, ~5- to 8-fold more FRCs were found in draining bLNs relative to naive mice. We observed similar response kinetics for LECs and BECs. In contrast, all three infections induced increased LN cellularity that peaked 7 days after infection. Thus, the LSC populations responded with different kinetics, presumably in response to infection-specific cues, yet all induced sustained expansion of FRCs and LECs that persisted for at least 30 days.

The marked changes in LSC gene expression induced by HSV infection were not sustained, resulting in transcriptional profiles at day 30 that were essentially indistinguishable from those of uninfected mice (Figure 2A). To investigate the significance of sustained LSC expansion for subsequent immune responses, we infected mice on the skin with HSV and 30 days later subjected the same mice to heterologous infection with VV or LCMV. Alternately, mice were first infected with VV and 30 days later challenged with HSV. In all combinations, FRCs, LECs, and BECs expanded with similar kinetics, peaking at day 15, whereas LN cellularity peaked at day 7 (Figure 5B). T cell responses and LN cellularity in naive or previously challenged mice were the same, indicating that the enlarged LN did not influence the magnitude of subsequent responses (Figure S5D). Moreover, the number of LSCs at the peak of infection, as well as LN cellularity, was the same during primary and secondary challenge. Furthermore, 30 days after the second infection, LSC populations contracted to levels equivalent to that at day 30 after primary infection, indicating that successive infections did not result in progressively larger LNs. Rather, the LNs were programmed with a new set point after an initial immune response that persisted with subsequent challenge.

Examination of the magnitude of FRC expansion during primary versus secondary heterologous infections revealed that "experienced" LNs expanded considerably less than naive LNs (Figure 5C). In particular, the extent of FRC expansion was substantially lower during secondary responses, demonstrating that less proliferation was required to reach the same peak level. Thus, prolonged LN hypertrophy sustained expansion of the FRC compartment after virus infection, and this altered LN stromal niche influenced the magnitude of remodeling during subsequent infection.

DISCUSSION

The marked changes in LN size and organization during immune responses are controlled by subsets of stromal cells that construct and support the tissue. We describe a comprehensive analysis of LSC responses to infection. LN FRCs, LECs, and BECs proliferated and expanded in number significantly after skin HSV, VV, and LCMV infection. The kinetics of LSC expansion induced by the different pathogens was distinct, yet by 1 month post-infection, the numbers of $gp38^{+}$ FRCs were similar between each infection group. Transcriptomic analysis of LSCs revealed that coordinate regulation of large numbers of genes defined the stromal response to infection. Both shared and unique cohorts of genes were regulated in LSC subsets after HSV infection. Notably, gene expression in LSCs 30 days after infection was equivalent to that seen prior to infection, demonstrating that the stromal cells did not generate a transcriptional memory of the response. However, previously primed LNs sustained expanded FRC networks and supported subsequent responses via reduced stromal cell expansion. These data indicate that the requirement for LN remodeling is different in LNs previously exposed to pathogens, which has important implications for understanding LN remodeling in humans.

LN hypertrophy or lymphadenopathy accompanies infections, inflammation, and cancers. Recent studies have shown that immunization induces expansion of LSC subsets (Abe et al., 2014; Chyou et al., 2011; Denton et al., 2014; Yang et al., 2014). Inflammation induces an increase in the recruitment and retention of lymphocytes in LN and serves to increase the likelihood that rare naive T cells will encounter cognate antigen (Shiow et al., 2006; Soderberg et al., 2005), yet the degree to which such enlargement of LNs is required for the induction or maintenance of immune responses is not clear. After skin HSV-1 infection of mice, we observed rapid expansion of FRCs, LECs, and BECs,

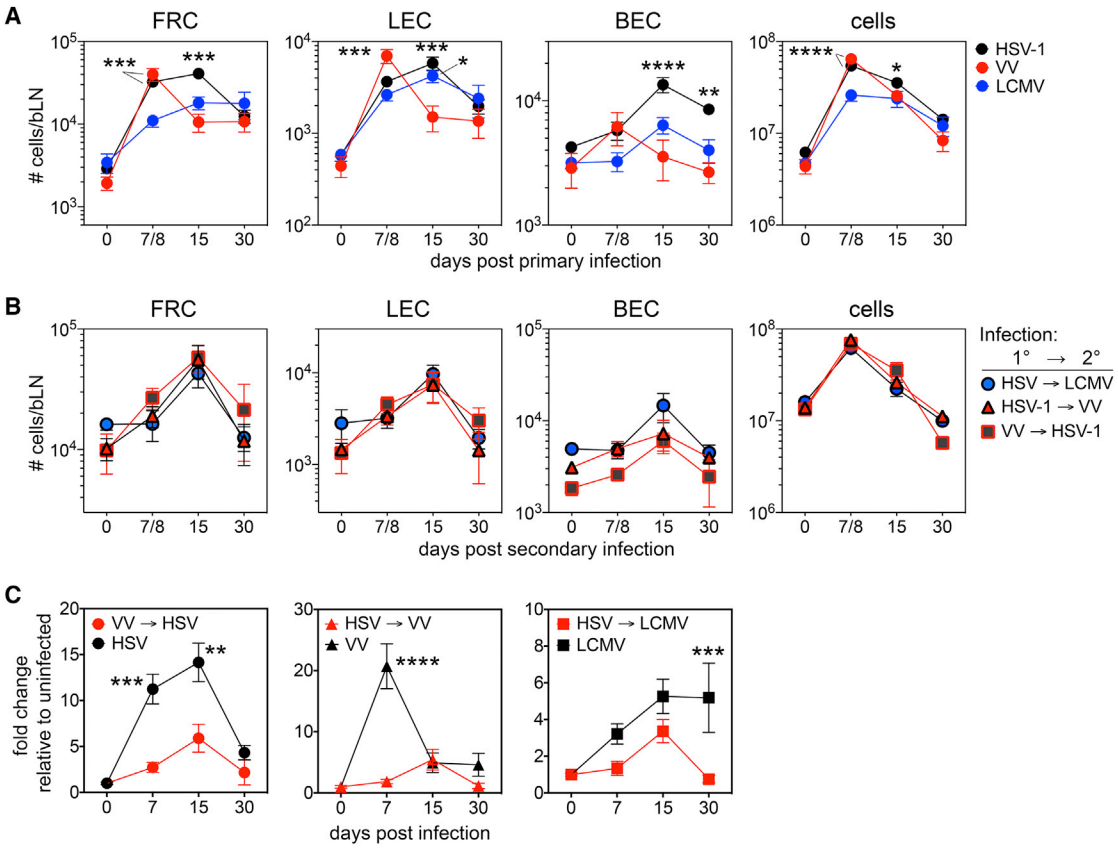

Figure 5. Altered Kinetics and Magnitude of LSC Responses during Secondary Infection

(A) Different kinetics of LSC expansion in response to skin infection with different viruses. Mice were infected on the scarified skin of the flank with either HSV, vaccinia virus (VV), or LCMV Armstrong and the draining bLN analyzed on days 7 (HSV or VV) or 8 (LCMV), 15, and 30. n = 8–22 mice per group.

(B) Heterologous infection induces similar kinetics of LSC expansion irrespective of viral pathogen. Mice were infected with either HSV, VV or LCMV on the skin of mice infected 30 days previously with either HSV, VV, or LCMV and the draining bLN analyzed on days 7 (HSV or VV) or 8 (LCMV), 15, and 30. n = 4–10 mice per group.

(C) Reduced expansion of FRCs following a second heterologous infection on the skin. Mice were infected with HSV, VV, or LCMV, with VV followed by HSV after 30 days, or with HSV followed by VV or LCMV after 30 days. FRC expansion in bLNs was analyzed at various times after infection and plotted relative to that prior to primary (black lines) or secondary (red lines) challenge. Data are pooled from two or three independent experiments.

Error bars represent mean ± SEM. *p < 0.05, **p < 0.01, ***p < 0.001, and ****p < 0.0001 by two-way ANOVA. See also Figure S5.

as well as PNAd^{+} BECs. This LSC expansion lagged behind the increase in immune cells within the LN, as observed previously (Denton et al., 2014; Yang et al., 2014). Conspicuously, skin infection with VV resulted in an earlier peak and contraction of LSCs, whereas LCMV infection induced relatively weak responses by FRCs. This implied that pathogen-derived signals were important for influencing the timing and magnitude of LSC responses to infection. We identified IFN-I as one signal mediating LSC expansion after infection, possibly via regulation of lymphocyte recruitment and retention (Shiow et al., 2006). However, we expect that multiple signals will contribute to this process, dependent upon the amount and type of inflammation induced by individual pathogens.

Recruitment of T and B cells controlled expansion of the bLN LSCs after infection, similar to that after immunization (Yang et al., 2014). We found that preventing the entry of immune cells into LNs by integrin blockade after infection was sufficient to inhibit FRC expansion, although it remains possible that integrin-mediated interactions also contribute to this response. RAG$^{-/-}$ mice showed no LSC expansion, and μMT$^{-/-}$ mice had reduced responses, yet TCR-α$^{-/-}$ mice were largely normal. We could restore LSC expansion in RAG$^{-/-}$ mice by adoptive transfer of T or B cells, yet only B cells were capable of sustaining responses for longer than 1 week. Prior reports have shown that expansion of LN lymphatics and vasculature can be controlled by B cells (Angeli et al., 2006; Kumar et al., 2010), a process that required lymphotoxin LT-αβ expression by B cells. We do not yet know whether B cells also sustain FRC responses after infection in an LT-αβ-dependent manner. Remodeling of LN medullary regions during inflammation was also shown to require B cells and involve LT-αβ signals (Abe et al., 2014). We observed similar changes after HSV infection and a sustained increase in gp38^{+} FRCs in the medulla. Although we could not distinguish medullary FRCs by flow cytometry, it will be important to determine how this population contributes to responses in comparison to T cell zone FRCs.

Expression of gp38 was increased on FRCs and LECs, correlating with increased numbers of DCs in the bLNs. Recent reports have shown that DCs expressing Clec2 can overcome gp38-induced contractility in FRCs, permitting stretching of the stromal network (Acton et al., 2014; Astarita et al., 2015). This may facilitate very early expansion of LNs by relaxing the stromal network. However, once the FRCs proliferate, upregulation of gp38 might be required to enforce FRC contractility as the number of DCs increases. Since gp38 also influences DC migration (Acton et al., 2012) and maintains the integrity of HEVs (Herzog et al., 2013), upregulation of gp38 during inflammation and LN expansion could ensure such processes are preserved. DCs were also shown to promote FRC survival during immune responses via gp38 upregulation (Kumar et al., 2015). All LSC subsets also increased expression of versican. Overexpression of versican in human dermal fibroblasts can lead to increased SMA expression and enhanced cell contractility (Hattori et al., 2011), suggesting that this might also help to sustain the integrity of the LSC networks during LN expansion.

We describe the transcriptional signatures of LSC subsets during infection. The number of genes regulated by FRCs, LECs, and BECs after infection was surprising. In particular, FRCs and LECs each up- or downregulated more than 1,000 genes. We identified numerous immune-related genes in each subset that were increased after infection. All three LSC subsets upregulated the chemokine Cxcl9, which can play important roles in T cell responses. The LSC subsets also increased expression of various MHC II genes and showed increased cell surface expression, particularly on FRCs. MHC II complexes acquired by LSCs from DCs can contribute to T cell peripheral tolerance (Dubrot et al., 2014), while LSC MHC II expression may also contribute to regulatory T cell maintenance (Baptista et al., 2014). Whether increased MHC II expression during immune responses can influence T cell responses will be important to assess.

The LN LSCs also regulated multiple cytokine and chemokine genes after infection. Our data suggest that FRCs are a prominent source of IL-33 in LNs after infection. IL-33 has been shown to be important for CTL responses after LCMV and murine γ-herpesvirus 68 infection (Bonilla et al., 2012). Additionally, many genes involved in cellular adhesion, cytoskeleton, extracellular matrix, metabolism, and cell growth were transcriptionally regulated by LSCs, as well as numerous transcription factors, including those involved in inflammation and cytokine signaling. These transcriptional signatures will be important for dissection of the roles of LSCs in LN expansion and immune responses.

We were surprised to find that gene expression in all LSC subsets returned to homeostatic levels within 30 days of infection, without any "memory" signature. This demonstrates that infection did not induce differentiation of the LSCs, at least at the population level. Further, this shows that LSCs can quickly establish quiescence after infection, despite maintaining increased populations, particularly in the case of FRCs. The LSC response to infection also contrasts with transcriptional changes induced in FRCs in tumor draining LNs, where fewer and considerably more modest gene expression changes were observed (Riedel et al., 2016). However, both infection and tumors regulated genes, including *Thy1*, *Aqp1*, *Cyp2f2*, and *Ccl21*, in FRCs, suggesting that these are programmed pathways important to support immune responses. In particular, CCL21 downregulation may support immune responses.

The amplified populations of LN FRCs were sustained for at least 3 months after infection, suggesting that the initial remodeling of naive LNs by infection lastingly altered the cellular architecture. Furthermore, we found that after a second unrelated infection, LSC expansion did not exceed the maximal level observed during the primary infection. Thus, a hallmark of LSC responses in experienced LNs was reduced expansion, potentially placing less physical and metabolic stress on the tissue to achieve the same outcome. Moreover, the FRCs and LECs contracted to the new baseline set by the primary infection, and the total cellularity of these LN remained largely unchanged, as previously described following multiple heterologous prime-boost vaccinations (Vezys et al., 2009).

Thus, our experiments reveal that an immune response can induce prolonged changes in LNs that may support subsequent immune challenges through boosted stromal cell populations. Recent experiments have shown the influence of broad microbial exposure on the cells of the immune system (Beura et al., 2016), suggesting that this may also translate to remodeling of the lymphoid tissues. As such, the LSC responses to heterologous infections we describe here may be more akin to LN remodeling in humans, since we are regularly exposed to microbes. It will be important to ascertain how different human pathogens alter stromal cell responses to potentially identify novel pathways for boosting immune responses.

EXPERIMENTAL PROCEDURES

Mice and Infections

C57BL/6, gBT-I (Mueller et al., 2002), gDT-II, FABP7$^{-/-}$ (Tokuda et al., 2010), OBI.RAG$^{-/-}$ (Dougan et al., 2012), IFN-αR2$^{-/-}$, RAG1/Je$^{-/-}$, TCR-α$^{-/-}$, μMT$^{-/-}$, ICE$^{-/-}$, TLR3$^{-/-}$, TRIF$^{-/-}$, MyD88$^{-/-}$, IRF8$^{-/-}$, IL-15$^{-/-}$, and IFN-γ$^{-/-}$ mice were bred in the Department of Microbiology and Immunology. gBT-I and gDT-II mice expressing T cell receptors recognizing the HSV-1 glycoprotein B-derived epitope $gB_{498-505}$ and glycoprotein D-derived epitope $gD_{315-327}$, respectively. Animal experiments were approved by The University of Melbourne Animal Ethics Committee.

Virus Infections

Mice were infected on the skin of the flank with either 10^6 plaque-forming units (PFUs) of HSV-1 (KOS) or vaccinia virus (CR-19) or 10^4 PFUs of LCMV (Armstrong) by scarification. Mice were anaesthetized by intraperitoneal (i.p.) injection of a 1:1 mixture of ketamine and Xylazil (10 μL/g body weight). Hair was removed from the left flank of each mouse with clippers and depilation cream (Veet, Reckitt Benckiser) and a small area of skin (2–4 mm^2) corresponding with the top of the spleen was lightly abraded using a Dremel power tool and bullet-shaped sanding tip before inoculation of virus in a 10 μL volume. The infection site was then covered with a piece of OpSite Flexigrid and secured with Micropore tape and Transpore tape (3M) for 48 hr following infection. For secondary infections, mice were infected with 10^6 PFUs of HSV-1 or vaccinia virus or 10^4 PFUs of LCMV 30 days after primary infection.

Stromal Cell Isolation and Flow Cytometry

Brachial and inguinal lymph nodes were harvested, teased apart with forceps, and incubated at 37°C in RPMI containing 1.5 mg/mL Collagenase D (Roche), 0.1 mg/ml DNase (Sigma), and 5% fetal calf serum (FCS) for 20 min. Tissues were incubated for a further 15 min at 37°C with the addition of 0.8 mg/mL Dispase (Roche) and re-suspended every 5 min. Remaining tissue pieces were further digested in fresh digest medium for 10 min. Single-cell suspensions

were then stained with antibodies for flow cytometry. The following antibodies from BD Biosciences were used: fluorescein isothiocyanate (FITC)-conjugated CD8 (53-6.7, 1/400), allophycocyanin (APC)-conjugated CD45.1 (A20, 1/200) and CD45.2 (104, 1/100), phycoerythrin (PE)-conjugated CD4 (RM4-4, 1/300), Alexa-Fluor-700-conjugated major histocompatibility complex class II (IA/IE) (M5/114.15.2, 1/200), PE-conjugated gp38 (8.1.1, 1/200), Alexa-488-conjugated HEVs (MECA 79, 1/200), PE Cy7-conjugated CD31 (MEC 13.3, 1/200), PE Cy7-conjugated CD11c (N418, 1/400), APC-conjugated CD19 (1D3, 1/100), APC-conjugated CD21/35 (7G6, 1/100), and APC-conjugated BrdU (1/50); purified CD16/32 (2.4G2, 1/200) was used to block nonspecific Fc receptor binding. Propidium iodide was used to exclude dead cells. FACSCanto II (BD) and FlowJo software (TreeStar) packages were used for analysis.

For cell sorting, cell suspensions were first depleted of $CD45^+$ cells utilizing $CD45^+$ magnetic-activated cell sorting (MACS) beads according to the manufacturer's instructions (Miltenyi Biotec). Cells were stained for CD45, gp38, CD31, and CD21/35 to exclude FDCs. On average, less than 1% of $gp38^+$ cells were $CD21/35^+$ in naive mice. An FACSAria III (BD) was used for sorting using a 100-μm nozzle at 20 psi.

Gene Expression Microarrays

Stromal cell subsets from bLN were sorted into RPMI containing 10% FCS, immediately collected by centrifugation, snap frozen in liquid N_2, and stored at −80°C after cell sorting. RNA was isolated utilizing the RNAeasy kit (QIAGEN) according to manufacturer's instructions. RNA quality and quantity was assessed with a Bioanalyzer 2100 (Agilent) and an RNA 6000 Pico kit (Agilent). RNA was subsequently amplified and converted into cDNA by a linear amplification method with the WT-Ovation Pico System (Nugen), the cDNA was labeled with the Encore Biotin module (Nugen) and hybridized to GeneChip MouseGene 1.0 ST chips (Affymetrix) at the Molecular Genomics Core Facility of the Peter MacCallum Cancer Centre in Australia.

Bioinformatics analysis used Bioconductor software (Huber et al., 2015). Microarray intensities were background corrected, normalized, and summarized by probe set using robust multi-array analysis (RMA) (Irizarry et al., 2003). Probe-set annotation was obtained from the Affymetrix file "MoGene-1_0-st-v1.na31.mm9.transcript.csv" and from the org.Mm.eg.db annotation package. Control probe sets were removed. Probe sets were retained for downstream analysis if they were in the top 75% of intensities in three or more samples. Differential expression analysis was undertaken using linear modeling in the limma software package (Ritchie et al., 2015). Correlation between samples from the same cell sort was modeled using limma's duplicate correlation function (Smyth et al., 2005). Differential expression was assessed using TREAT empirical Bayes t tests relative to a fold change threshold of 1.1 (McCarthy and Smyth, 2009) and the FDR was controlled at 5%. The TREAT method requires genes to have expression changes significantly above the specified threshold. For this study, the statistically significant fold changes were almost all (97%) greater than 1.5-fold and most greater than 2-fold. Multi-dimensional scaling plots were drawn using limma's plotMDS function using leading fold change distances.

qRT-PCR

For qRT-PCR analysis of the expression of *Fabp7* and *Ccl21*, RNA was extracted with an RNeasy Micro Kit (QIAGEN), and cDNA was synthesized with SuperScript III Reverse Transcriptase (Invitrogen) and oligo(dT) primers (Promega). Fast SYBR green Master mix (Life Technologies) was used for qRT-PCR. Primer sequences were 5′-GGGTAAGACCCGAGTTCCTC-3′ and 5′-GAGCTTGTCTCCATCCAACC-3′ for *Fabp7* and 5′-ATCCCGGCAA TCCTGTTCTC-3′ and 5′-GGTTCTGCACCCAGCCTTC-3′ for *Ccl21*. Expression for each sample was calculated by the $2^{-\Delta Ct}$ method.

Adoptive Transfer of Lymphocytes

Naive gBT-I.Ly5.1 and gDT-II.Ly5.1 cells were isolated from LN and spleen, and gDT-II cells were further enriched by positive and negative selection using magnetic beads, as described previously (Hor et al., 2015). T or B cells were enriched from pooled LN and spleens of naive B6 mice using MACS beads. Naive mice received gBT-I.Ly5.1 and gDT-II.Ly5.1 cells, enriched T cells or B cells, or suspensions of LN cells intravenously via the tail vein (see figure legends for the number of cells transferred). In-vitro-activated gBT-I effector cells were activated by peptide-pulsed splenocytes as previously described (Mackay et al., 2012), and 5×10^4 cells were injected intravenously 3 days post-HSV-1 infection.

Integrin Blockade and BrdU Labeling

To block entry of lymphocytes to the LN, mice received 100 μg of the function-blocking antibodies to the integrins α4 (PS/2) and αL (M17/4) on days 1, 3, and 5 post-infection via i.p. injection. To assess proliferation of stromal cell populations, mice received 0.25 mg/mL BrdU (BD Biosciences) via i.p. injection followed by continuous labeling with BrdU in drinking water (0.8 mg/mL) for the periods days 0–7, days 7–11, and 11–15 post-infection.

ELISA

Tissues were removed from mice and placed in PBS supplemented with 1% BSA and 10 μL/mL protease inhibitor cocktail P8340 (Sigma-Aldrich). Tissue was homogenized and supernatant used for ELISA. Detection of mouse CCL21 was performed using a DuoSet ELISA development kit (R&D Systems) as per the manufacturer's instructions.

Immunofluorescence and Confocal Microscopy

Lymph nodes were harvested and fixed in periodate-lysine-paraformaldehyde (PLP) fixative for 4–8 hr, incubated in 20% sucrose overnight at 4°C. Tissue sections were cut at 6 μm thickness with a cryostat (Leica CM3050S) and air-dried before being fixed in acetone for 5 min, dried, and then blocked for 20 min (Protein Block X0909, DAKO) at room temperature (RT). Sections were then stained with primary antibodies for 1.5 hr, washed in PBS for 10 min, and stained with secondary antibodies for 30 min. Images were acquired with an LSM710 confocal microscope (Carl Zeiss) and processed with Imaris (Bitplane) and Photoshop (Adobe). The following antibodies were used: Alexa-Fluor-647-conjugated B220 (1/100), Alexa-Fluor-405-conjugated CD3 (1/100), Alexa-488-conjugated CD31 (1/200), Alexa-Fluor-647-conjugated Ki67 (1/200), Alexa-488-conjugated HEV (1/200), polyclonal anti-LYVE-1 (1/400), and anti-podoplanin (8.1.1, supernatant). Appropriate secondary antibodies from Life Technologies were Alexa Fluor goat anti-hamster 568 (1/1,000), donkey anti-rabbit 647 (1/1,000), and donkey anti-rat 488 (1/1,000).

Statistical Analysis

Graphs were plotted using Prism 5 (GraphPad), and comparison of datasets was performed by one- or two-way analysis of variance, or Mann-Whitney t tests, as indicated. All graphs depict means ± SEM. The appropriate statistical methods were chosen according to experimental setup and data distribution. Sample sizes were chosen on the basis of previous experiences with the relevant experimental models.

ACCESSION NUMBERS

The accession number for the microarray data reported in this paper is GEO: GSE84284 (http://www.ncbi.nlm.nih.gov/geo/).

SUPPLEMENTAL INFORMATION

Supplemental Information includes five figures and two tables and can be found with this article online at http://dx.doi.org/10.1016/j.celrep.2016.12.038.

AUTHOR CONTRIBUTIONS

J.L.G., A.W., Y.O.A., J.L.H., and S.D. performed experiments. R.L., J.Z.M., and G.K.S. carried out microarray analysis. N.T. and Y.O. supplied reagents. L.K.M. and W.R.H. contributed to analysis. S.N.M. designed the study and wrote the manuscript. All authors edited and approved the final manuscript.

ACKNOWLEDGMENTS

We thank Rafi Ahmed (Emory University, GA) for LCMV virus, Weisan Chen (La Trobe University) for vaccinia virus (which was originally a gift from Jonathan

Yewdell and Jack Bennink [NIH, Bethesda, MD]), Michael Hickey (Monash University) for PS/2 and M17/4 antibodies, and Hidde Ploegh (Whitehead Institute, Cambridge, MA) for OBI mice. This work was supported by the Australian Research Council (DP140101246).

Received: September 13, 2016
Revised: November 5, 2016
Accepted: December 12, 2016
Published: January 10, 2017

REFERENCES

Abe, J., Shichino, S., Ueha, S., Hashimoto, S., Tomura, M., Inagaki, Y., Stein, J.V., and Matsushima, K. (2014). Lymph node stromal cells negatively regulate antigen-specific CD4+ T cell responses. J. Immunol. *193*, 1636–1644.

Acton, S.E., Astarita, J.L., Malhotra, D., Lukacs-Kornek, V., Franz, B., Hess, P.R., Jakus, Z., Kuligowski, M., Fletcher, A.L., Elpek, K.G., et al. (2012). Podoplanin-rich stromal networks induce dendritic cell motility via activation of the C-type lectin receptor CLEC-2. Immunity *37*, 276–289.

Acton, S.E., Farrugia, A.J., Astarita, J.L., Mourão-Sá, D., Jenkins, R.P., Nye, E., Hooper, S., van Blijswijk, J., Rogers, N.C., Snelgrove, K.J., et al. (2014). Dendritic cells control fibroblastic reticular network tension and lymph node expansion. Nature *514*, 498–502.

Angeli, V., Ginhoux, F., Llodrà, J., Quemeneur, L., Frenette, P.S., Skobe, M., Jessberger, R., Merad, M., and Randolph, G.J. (2006). B cell-driven lymphangiogenesis in inflamed lymph nodes enhances dendritic cell mobilization. Immunity *24*, 203–215.

Astarita, J.L., Cremasco, V., Fu, J., Darnell, M.C., Peck, J.R., Nieves-Bonilla, J.M., Song, K., Kondo, Y., Woodruff, M.C., Gogineni, A., et al. (2015). The CLEC-2-podoplanin axis controls the contractility of fibroblastic reticular cells and lymph node microarchitecture. Nat. Immunol. *16*, 75–84.

Bajénoff, M., Glaichenhaus, N., and Germain, R.N. (2008). Fibroblastic reticular cells guide T lymphocyte entry into and migration within the splenic T cell zone. J. Immunol. *181*, 3947–3954.

Baptista, A.P., Roozendaal, R., Reijmers, R.M., Koning, J.J., Unger, W.W., Greuter, M., Keuning, E.D., Molenaar, R., Goverse, G., Sneeboer, M.M., et al. (2014). Lymph node stromal cells constrain immunity via MHC class II self-antigen presentation. eLife *3*, 04433.

Beura, L.K., Hamilton, S.E., Bi, K., Schenkel, J.M., Odumade, O.A., Casey, K.A., Thompson, E.A., Fraser, K.A., Rosato, P.C., Filali-Mouhim, A., et al. (2016). Normalizing the environment recapitulates adult human immune traits in laboratory mice. Nature *532*, 512–516.

Bonilla, W.V., Fröhlich, A., Senn, K., Kallert, S., Fernandez, M., Johnson, S., Kreutzfeldt, M., Hegazy, A.N., Schrick, C., Fallon, P.G., et al. (2012). The alarmin interleukin-33 drives protective antiviral CD8$^+$ T cell responses. Science *335*, 984–989.

Brown, F.D., and Turley, S.J. (2015). Fibroblastic reticular cells: organization and regulation of the T lymphocyte life cycle. J. Immunol. *194*, 1389–1394.

Chyou, S., Benahmed, F., Chen, J., Kumar, V., Tian, S., Lipp, M., and Lu, T.T. (2011). Coordinated regulation of lymph node vascular-stromal growth first by CD11c+ cells and then by T and B cells. J. Immunol. *187*, 5558–5567.

Cremasco, V., Woodruff, M.C., Onder, L., Cupovic, J., Nieves-Bonilla, J.M., Schildberg, F.A., Chang, J., Cremasco, F., Harvey, C.J., Wucherpfennig, K., et al. (2014). B cell homeostasis and follicle confines are governed by fibroblastic reticular cells. Nat. Immunol. *15*, 973–981.

Denton, A.E., Roberts, E.W., Linterman, M.A., and Fearon, D.T. (2014). Fibroblastic reticular cells of the lymph node are required for retention of resting but not activated CD8+ T cells. Proc. Natl. Acad. Sci. USA *111*, 12139–12144.

Dougan, S.K., Ogata, S., Hu, C.C., Grotenbreg, G.M., Guillen, E., Jaenisch, R., and Ploegh, H.L. (2012). IgG1+ ovalbumin-specific B-cell transnuclear mice show class switch recombination in rare allelically included B cells. Proc. Natl. Acad. Sci. USA *109*, 13739–13744.

Dubrot, J., Duraes, F.V., Potin, L., Capotosti, F., Brighouse, D., Suter, T., LeibundGut-Landmann, S., Garbi, N., Reith, W., Swartz, M.A., and Hugues, S. (2014). Lymph node stromal cells acquire peptide-MHCII complexes from dendritic cells and induce antigen-specific CD4$^+$ T cell tolerance. J. Exp. Med. *211*, 1153–1166.

Fletcher, A.L., Lukacs-Kornek, V., Reynoso, E.D., Pinner, S.E., Bellemare-Pelletier, A., Curry, M.S., Collier, A.-R., Boyd, R.L., and Turley, S.J. (2010). Lymph node fibroblastic reticular cells directly present peripheral tissue antigen under steady-state and inflammatory conditions. J. Exp. Med. *207*, 689–697.

Fletcher, A.L., Acton, S.E., and Knoblich, K. (2015). Lymph node fibroblastic reticular cells in health and disease. Nat. Rev. Immunol. *15*, 350–361.

Gretz, J.E., Norbury, C.C., Anderson, A.O., Proudfoot, A.E., and Shaw, S. (2000). Lymph-borne chemokines and other low molecular weight molecules reach high endothelial venules via specialized conduits while a functional barrier limits access to the lymphocyte microenvironments in lymph node cortex. J. Exp. Med. *192*, 1425–1440.

Hattori, N., Carrino, D.A., Lauer, M.E., Vasanji, A., Wylie, J.D., Nelson, C.M., and Apte, S.S. (2011). Pericellular versican regulates the fibroblast-myofibroblast transition: a role for ADAMTS5 protease-mediated proteolysis. J. Biol. Chem. *286*, 34298–34310.

Herzog, B.H., Fu, J., Wilson, S.J., Hess, P.R., Sen, A., McDaniel, J.M., Pan, Y., Sheng, M., Yago, T., Silasi-Mansat, R., et al. (2013). Podoplanin maintains high endothelial venule integrity by interacting with platelet CLEC-2. Nature *502*, 105–109.

Hirose, J., Kawashima, H., Yoshie, O., Tashiro, K., and Miyasaka, M. (2001). Versican interacts with chemokines and modulates cellular responses. J. Biol. Chem. *276*, 5228–5234.

Hor, J.L., Whitney, P.G., Zaid, A., Brooks, A.G., Heath, W.R., and Mueller, S.N. (2015). Spatiotemporally distinct interactions with dendritic cell subsets facilitates CD4+ and CD8+ T cell activation to localized viral infection. Immunity *43*, 554–565.

Huber, W., Carey, V.J., Gentleman, R., Anders, S., Carlson, M., Carvalho, B.S., Bravo, H.C., Davis, S., Gatto, L., Girke, T., et al. (2015). Orchestrating high-throughput genomic analysis with Bioconductor. Nat. Methods *12*, 115–121.

Irizarry, R.A., Bolstad, B.M., Collin, F., Cope, L.M., Hobbs, B., and Speed, T.P. (2003). Summaries of Affymetrix GeneChip probe level data. Nucleic Acids Res. *31*, e15.

Khan, O., Headley, M., Gerard, A., Wei, W., Liu, L., and Krummel, M.F. (2011). Regulation of T cell priming by lymphoid stroma. PLoS ONE *6*, e26138.

Kumar, V., Scandella, E., Danuser, R., Onder, L., Nitschké, M., Fukui, Y., Halin, C., Ludewig, B., and Stein, J.V. (2010). Global lymphoid tissue remodeling during a viral infection is orchestrated by a B cell-lymphotoxin-dependent pathway. Blood *115*, 4725–4733.

Kumar, V., Dasoveanu, D.C., Chyou, S., Tzeng, T.C., Rozo, C., Liang, Y., Stohl, W., Fu, Y.X., Ruddle, N.H., and Lu, T.T. (2015). A dendritic-cell-stromal axis maintains immune responses in lymph nodes. Immunity *42*, 719–730.

Link, A., Vogt, T.K., Favre, S., Britschgi, M.R., Acha-Orbea, H., Hinz, B., Cyster, J.G., and Luther, S.A. (2007). Fibroblastic reticular cells in lymph nodes regulate the homeostasis of naive T cells. Nat. Immunol. *8*, 1255–1265.

Lukacs-Kornek, V., Malhotra, D., Fletcher, A.L., Acton, S.E., Elpek, K.G., Tayalia, P., Collier, A.-R., and Turley, S.J. (2011). Regulated release of nitric oxide by nonhematopoietic stroma controls expansion of the activated T cell pool in lymph nodes. Nat. Immunol. *12*, 1096–1104.

Luther, S.A., Tang, H.L., Hyman, P.L., Farr, A.G., and Cyster, J.G. (2000). Coexpression of the chemokines ELC and SLC by T zone stromal cells and deletion of the ELC gene in the plt/plt mouse. Proc. Natl. Acad. Sci. USA *97*, 12694–12699.

Mackay, L.K., Stock, A.T., Ma, J.Z., Jones, C.M., Kent, S.J., Mueller, S.N., Heath, W.R., Carbone, F.R., and Gebhardt, T. (2012). Long-lived epithelial immunity by tissue-resident memory T (TRM) cells in the absence of persisting local antigen presentation. Proc. Natl. Acad. Sci. USA *109*, 7037–7042.

Malhotra, D., Fletcher, A.L., Astarita, J., Lukacs-Kornek, V., Tayalia, P., Gonzalez, S.F., Elpek, K.G., Chang, S.K., Knoblich, K., Hemler, M.E., et al.; Immunological Genome Project Consortium (2012). Transcriptional profiling of stroma

from inflamed and resting lymph nodes defines immunological hallmarks. Nat. Immunol. *13*, 499–510.

McCarthy, D.J., and Smyth, G.K. (2009). Testing significance relative to a fold-change threshold is a TREAT. Bioinformatics *25*, 765–771.

Mueller, S.N., and Germain, R.N. (2009). Stromal cell contributions to the homeostasis and functionality of the immune system. Nat. Rev. Immunol. *9*, 618–629.

Mueller, S.N., Heath, W., McLain, J.D., Carbone, F.R., and Jones, C.M. (2002). Characterization of two TCR transgenic mouse lines specific for herpes simplex virus. Immunol. Cell Biol. *80*, 156–163.

Mueller, S.N., Hosiawa-Meagher, K.A., Konieczny, B.T., Sullivan, B.M., Bachmann, M.F., Locksley, R.M., Ahmed, R., and Matloubian, M. (2007). Regulation of homeostatic chemokine expression and cell trafficking during immune responses. Science *317*, 670–674.

Riedel, A., Shorthouse, D., Haas, L., Hall, B.A., and Shields, J. (2016). Tumor-induced stromal reprogramming drives lymph node transformation. Nat. Immunol. *17*, 1118–1127.

Ritchie, M.E., Phipson, B., Wu, D., Hu, Y., Law, C.W., Shi, W., and Smyth, G.K. (2015). limma powers differential expression analyses for RNA-sequencing and microarray studies. Nucleic Acids Res. *43*, e47.

Schulz, O., Hammerschmidt, S.I., Moschovakis, G.L., and Förster, R. (2016). Chemokines and Chemokine Receptors in Lymphoid Tissue Dynamics. Annu. Rev. Immunol. *34*, 203–242.

Sharifi, K., Morihiro, Y., Maekawa, M., Yasumoto, Y., Hoshi, H., Adachi, Y., Sawada, T., Tokuda, N., Kondo, H., Yoshikawa, T., et al. (2011). FABP7 expression in normal and stab-injured brain cortex and its role in astrocyte proliferation. Histochem. Cell Biol. *136*, 501–513.

Shiow, L.R., Rosen, D.B., Brdicková, N., Xu, Y., An, J., Lanier, L.L., Cyster, J.G., and Matloubian, M. (2006). CD69 acts downstream of interferon-alpha/beta to inhibit S1P1 and lymphocyte egress from lymphoid organs. Nature *440*, 540–544.

Siegert, S., Huang, H.-Y., Yang, C.-Y., Scarpellino, L., Carrie, L., Essex, S., Nelson, P.J., Heikenwalder, M., Acha-Orbea, H., Buckley, C.D., et al. (2011). Fibroblastic reticular cells from lymph nodes attenuate T cell expansion by producing nitric oxide. PLoS ONE *6*, e27618.

Sixt, M., Kanazawa, N., Selg, M., Samson, T., Roos, G., Reinhardt, D.P., Pabst, R., Lutz, M.B., and Sorokin, L. (2005). The conduit system transports soluble antigens from the afferent lymph to resident dendritic cells in the T cell area of the lymph node. Immunity *22*, 19–29.

Smyth, G.K., Michaud, J., and Scott, H.S. (2005). Use of within-array replicate spots for assessing differential expression in microarray experiments. Bioinformatics *21*, 2067–2075.

Soderberg, K.A., Payne, G.W., Sato, A., Medzhitov, R., Segal, S.S., and Iwasaki, A. (2005). Innate control of adaptive immunity via remodeling of lymph node feed arteriole. Proc. Natl. Acad. Sci. USA *102*, 16315–16320.

Tokuda, N., Adachi, T., Adachi, Y., Higashi, M., Sharifi, K., Tuerxun, T., Sawada, T., Kondo, H., and Owada, Y. (2010). Identification of FABP7 in fibroblastic reticular cells of mouse lymph nodes. Histochem. Cell Biol. *134*, 445–452.

Vezys, V., Yates, A., Casey, K.A., Lanier, G., Ahmed, R., Antia, R., and Masopust, D. (2009). Memory CD8 T-cell compartment grows in size with immunological experience. Nature *457*, 196–199.

Wight, T.N. (2002). Versican: a versatile extracellular matrix proteoglycan in cell biology. Curr. Opin. Cell Biol. *14*, 617–623.

Yang, C.-Y., Vogt, T.K., Favre, S., Scarpellino, L., Huang, H.-Y., Tacchini-Cottier, F., and Luther, S.A. (2014). Trapping of naive lymphocytes triggers rapid growth and remodeling of the fibroblast network in reactive murine lymph nodes. Proc. Natl. Acad. Sci. USA *111*, E109–E118.

Zanotti, L., Angioni, R., Calì, B., Soldani, C., Ploia, C., Moalli, F., Gargesha, M., D'Amico, G., Elliman, S., Tedeschi, G., et al. (2016). Mouse mesenchymal stem cells inhibit high endothelial cell activation and lymphocyte homing to lymph nodes by releasing TIMP-1. Leukemia *30*, 1143–1154.